We are IntechOpen, the world's leading publisher of Open Access books
Built by scientists, for scientists

6,900
Open access books available

185,000
International authors and editors

200M
Downloads

154
Countries delivered to

Our authors are among the

TOP 1%
most cited scientists

12.2%
Contributors from top 500 universities

CLARIVATE ANALYTICS
BOOK CITATION INDEX
INDEXED

WEB OF SCIENCE™

Selection of our books indexed in the Book Citation Index
in Web of Science™ Core Collection (BKCI)

Interested in publishing with us?
Contact book.department@intechopen.com

Microtribological Behavior of Polymer-Nanoparticle Thin Film with AFM

Xue Feng Li[1], Shao Xian Peng[1] and Han Yan[2]
[1]School of Chemical and Environmental Engineering,
Hubei University of Technology, Wuhan
[2]School of Civil Engineering, Hubei University of Technology, Wuhan
China

1. Introduction

1.1 Polymer-CNT nanocomposits

Carbon nanotubes (CNTs) have attracted significant scientific attention because of their remarkable mechanical properties and many potential applications (Balani et al., 2008; Vail et al., 2009). The tribological properties of CNTs as reinforcement agent in metal-based composite were studied by a few groups (Meng et al., 2009; Pei et al., 2008). The results indicated that metal-CNT composite coating was better wear resistance and self-lubricity than the metal coating. Ni-carbon nanotubes composite coating has better wear resistance and self-lubricity than the Ni coating. The poor solubility characteristics of CNTs have hindered it as an additive to liquid lubricants (Decher, 1997). If CNTs were dispersed in liquid lubricants by some physical or mechanical ways, CNTs still assembled and presented in the form of cluster. The soft chains of polymer molecules are reasonable to consider anti-wear for its flexibilities, great interests have been aroused in the thin polymer films on solid surface for their application in lubrication. Meanwhile the existence of rigid rod-like segments in the films is expected to be beneficial to bearing applied loads. Recently some chemists have adopted chemistry method for the preparation of soluble carbon nanotubes containing polymer (Riggs et al., 2000; Shaffer & Koziol, 2002). Attachment of surface polymer chain is expected to provide much more effective performance of nanocomposite materials, as dictated by the nature of the polymer. A lot of reports have described the attachment of short chains to CNTs to improve the performance of nanocomposite materials by esterification / amidation of surface acid groups like the preparation of poly(ethylene glycol)-carbon nanotubes (PEG-CNTs) described in the chapter (Chen et al., 1998; Li et al., 2011; Liu et al., 1998). However, very a few studies have been conducted in the grafting of CNTs by free radical polymerization, even though it is the commonest synthesis method and there are a lot of choices on the monomers and initiators. Exceptions include the attachment of prepolymerised poly(methyl methacrylate) and the formation of polystyrene grafted CNTs (Jia et al., 1999; Shaffer & Koziol, 2002). Here we report the synthesis of individual polyacrylamide-carbon nanotube (PAM-CNT) copolymer by an in-situ UV radiation initiated polymerization and water-soluble poly(vinyl alcohol)-carbon nanotube (PVA-CNT) copolymer by an in-situ radical initiated emulsion polymerization (Li et al.,

2004). Composite thin films were obtained by spin casting the copolymer aqueous solution onto freshly cleaved mica. The microtribological properties of the films were initial investigated using atomic force microscopy / friction force microscopy (AFM/FFM).

1.2 Diazoresin-nanoparticle self-assembly films

Another class of technologies known as self-assemble has very interesting applications in area of nano-composites and optoelectronic materials (Kwon et al., 2007). The self-assembly technique is exhibited to be a rapid and easy way to obtain molecular assemblies with precise control of composition which can be used in a wide variety of technologies ranging from microelectronic, corrosion protection and adhesion to electrochemistry, etc (Bai & Cheng, 2006; Kim et al., 2007). Tribological properties in microscales between two sliding solid surfaces are essential to supply super lubrication for micro-electro-mechanical systems (MEMS) (Cheng et al., 2006; Zhao et al., 2009). Therefore, the process of self-assembly films is considered critical technology for the realization of nano-scale devices (Bhushan et al., 2002; Medintz et al., 2005).

Since Cao's pioneering work, the covalently attached self-assembly films from diazoresin (DR) and different negatively charged materials have been prepared (Lu et al., 2004; Yang et al., 2005). This method, usually involving the alternate of two oppositely charged components on a substrate such as mica, silica wafer from aqueous solution, is environmentally friendly and easy in processing and does not require specific equipment. Nevertheless, studies on converting the physical force into covalent bonds to link the orderly carbon nanotubes / polymer thin films have seldom been reported. We describe a preparation method of poly (acrylic acid)-carbon nanotubes (PAA-CNTs), and a fabrication process of multilayer thin films constructed from PAA-CNTs and DR via a layer-by-layer technique, then the linkage bonds are converted under UV irradiation (Li et al., 2011). By this way, we also describe a preparation method of poly (acrylic acid)-titanium oxide (PAA-TiO$_2$) and poly (acrylic acid)-ferric hydroxide (PAA-Fe(OH)$_3$) sol, and a fabrication process of multilayer thin films constructed from PAA-TiO$_2$ and DR or PAA-Fe(OH)$_3$ and DR via a layer-by-layer technique (Li et al., 2009, 2011).

Then decomposition of the diazonium group could be detected after exposed under UV irradiation which leading to the conversion from ionic bond to covalent bond. In addition, to study surface morphology and friction of thin films on micro-scales, AFM and FFM are considered as excellent tools.

2. Experimental

2.1 Synthesis and microtribology of polymer-CNT nanocomposits

2.1.1 Synthesis PEG-CNT nanocomposites

Multi-wall CNTs were produced via the chemical vapor deposition method and purified using methods similar to those reported in the literatures (Hiura et al., 1995; Tsang et al., 1994). For example, CNT samples (300 mg) were suspended in an aqueous solution of hydrofluoric acid (20 wt.%, 60 ml) to prolonged sonication for 5 h and filtrated. The remaining solids were washed repeatedly with distilled water. The CNT samples thus were refluxed with an aqueous solution of nitric acid (22 wt.%, 60 ml) for 10 h. The mixture was centrifuged, and the remaining solids were washed repeatedly with distilled water many times, until the pH value

of CNT solution approached 7, and then dried in a vacuum oven to eliminate impurities. CNT sample was treated with HNO_3 solution to attach the carboxylic acid groups on the CNT surface, followed by treatment in thionyl chloride to convert the carboxylic acid into acyl chlorides. These functionalized CNTs can be grafted PEG by esterification.

2.1.2 Preparation of PVA-CNT copolymer

A typical preparation process of PVA-CNTs is as follows: the mixture of 10 ml of vinyl acetate, 50 ml distilled water, 100 mg sodium dodecylsulfate, 0.1 ml emulsifier OP-10 and 50 mg potassium persulfate (initiator) was charged into a 250 ml reaction flask. The mixture was emulsified by continuous stirring for 1.5 h at 65℃. The 100 mg purified CNTs and 50 mg potassium persulfate were then added to the emulsion system. The emulsion was sonicated by an ultrasonic cleaner for 30 min, stirred for 2.5 h and maintained at 65℃. After that the emulsion was filtered to remove insoluble particles. After that 100 ml 13 wt.% of sodium chloride aqueous solution was added to precipitate the polymeric product and then dried under vacuum at 50℃ in a constant weight. The product was dissolved in methanol and saponified. The fractions were repeated re-suspension in water and centrifugation at 5000 rpm to sediment PVA-CNT products and remove all of the free PVA that was stably soluble in water. These samples of PVA-CNTs are, forming stable suspension in water.

2.1.3 Synthesis of PAM-CNT copolymer

Acrylamide was distilled under reduced pressure and sealed for preservation at low temperature. Typical PAM-CNT copolymer was prepared by UV radiation initiated polymerization. The mixtures of 5 g acrylamide and 30 ml distilled water containing 50 mg CNTs were added into a 100 ml quartz reaction flask. After ultrasonic dispersing for 30 min and adding 10 ml UV initiator solution including 30 mg diphenylketone, 30 mg benzoin and 0.1 ml triethanolamine, the mixtures were radiated and stirred for 1.5 h at room temperature and under the protection of N_2. The products were filtrated and dried in a vacuum oven at 50 ℃. Dried products were repeatedly extracted with water to obtain soluble fraction. The fraction was centrifuged at 5000 rpm to sediment the grafted CNT products. Repeated re-suspension in water and centrifugation was used to remove all of the free PAM that was stably soluble in water. These samples of PAM-CNTs are, forming stable suspension in water.

2.1.4 Characterization of nanocomposites

The PEG-CNT and PAM-CNT copolymer were characterized using FT-IR (Bruker Equindx 55). For transmission electron microscope (TEM, JEM 100CX) observations, PVA-CNT samples were dispersed in water, then scooped up onto a holey carbon micro-grid. The purified PAM-CNT copolymer was also characterized by UV-visible spectrometer (SHIMADZU UV-2250 UV-VISIBLE SPECTRIPHO METER) and fluorescence spectrometer (SHIMADZU DATA RECORDER DR-3).

2.1.5 Tribological and microtribological test of nanocomposites by AFM and FFM

The tribological measurements were carried out by an MQ-800 four-ball tribotester at a rotational speed of 1450 rpm and at a temperature of 20℃. The maximum non-seizure load (PB value) was obtained by GB3142-82, similar to ASTMD2783; Wear scar diameter (WSD)

was measured under a test duration of 30 min; The stainless steel balls used in the tests were made of GCR15(AISIE52100) bearing steel with the 64-66 surface HRC hardness and 0.012 μm of surface roughness Ra. At the end of each test, the average WSD on the three lower balls was determined using optical microscopy to an accuracy of 0.01 mm. Since triethandamine is widely used in the metalworking fluid as a multifunctional additive, 2 wt.% of triethandamine aqueous solution as the base stock. And another water-based fluid with certain load-carrying and anti-wear properties, 0.5 wt.% OPZ (a type of water-soluble zinc alkoxyphosphate) fluid was chosen as the based stock (Duan, 1999). The different concentrations of PVA-CNTs prepared above were used as lubricant additive in the two kinds of base stock. WSD was measured for 30 min under a load of 200 N using the base stock without OPZ and 400 N using the base stock with OPZ respectively. The same concentration of the homopolymer reference additive was measured under the same condition.

The wear scar morphology was visualized with a JSM-35C scanning electron microscope (SEM) at a voltage of 25 kV. Specimens were wear scars on the steal balls in anti-wear tests which were performed at speed of 1450 rpm/min for 30 min, and were washed by alcohol and distilled water before inspection.

The Polymer-CNT aqueous solution (0.5 wt.%) was filtered through a 0.45 μm Teflon filter. Freshly cleaved micas were used as substrates. Thin films were obtained by spin casting (100 rpm, 1.5 min) the solution onto the mica substrates, and then dried in ambient temperature 2 days before used.

The measurements were performed with a Nanoscope a (Digital Instrument Inc.) equipped with a bioscopy G scanner (90μm) in contact mode and tapping mode. A commercial silicon cantilever (MikroMasch, Estonia, Russian) with triangular shape and force constant of K =0.12 N•m^{-1} were used. The images were obtained in air at 20 ℃ and relative humidity 50 % with 1 Hz scan rates.

Roughness images and root mean square (RMS) were obtained simultaneously when the scan angle was 0o. Friction images in trace and retrace scan directions were recorded when the scan angle was 90o. The applied load including the intrinsic adhesive force on thin films was calculated from set-point and "Force – Distance" curve .The applied load was changed and then the friction signals recorded, and so on, the friction-load figure was obtained (Li et al., 1999; Martínez-Martínez et al., 2009).

2.2 Fabrication and microtribology of diazoresin-nanoparticle self-assembly films

2.2.1 Preparation of PAA-CNTs

Acrylic acid (AA) was distilled under reduced pressure, dried with CaCl$_2$ overnight, and sealed for preservation at low temperature. Benzoyl peroxide (BPO) was recrystallized by chloroform. Other chemicals and solvent were used as received.

In a typical polymerization, 4 ml AA was dissolved in 25 ml 1, 4-dioxane, 60 mg BPO was added to the solution under stirring. After they have been deoxygenated by bubbling dry nitrogen gas for 10 min, the solution was heated to 85 ℃ and kept for 2.5 h under N$_2$. The 10 mg purified CNTs and 30 mg BPO was then added to the solution. The solution was ultrasonic dispersed for 30 min and maintained at 85 ℃ for 14 h with stirring under protection of N$_2$. The crude products dried in a vacuum oven were dissolved in 20 ml ethanol and precipitated by

adding 200 ml petroleum ether, then filtered off. And the procedure was repeated twice. After the product was dried in a vacuum oven, a deep grey product was obtained. The products can be dissolved in polar solvents, such as water and methanol.

2.2.2 Preparation of PAA-TiO$_2$

Titanium dioxide (TiO$_2$) nanoparticles were prepared by tetrabutyl titanate hydrolysis as described in reference (Eremenko et al., 2001). Nano TiO$_2$ solid particles was 2.0 wt.% in the hydrosol. For TEM (HITACHI H-500, with a voltage of 80 kV) observations, samples were dispersed in water solution, and then scooped up onto holey carbon micro-grids. The distributions of TiO$_2$ particles in the hydrosol were determined by a particle size distribution analyzer (LB-550, HORIBA Inc.).

Potassium persulfate (K$_2$S$_2$O$_8$) was recrystallized by water. In a typical polymerization process of PAA-TiO$_2$, TiO$_2$ sol 2.50 g, acrylic acid 3 ml and deionized water 9 ml were mixed to make a solution under stirring and ultrasonic dispersing for 30 min. Then 6 mg K$_2$S$_2$O$_8$ was added under stirring. The solution was deoxygenated by bubbling dry nitrogen gas for 10 min, then heated to 85 centigrade and kept for 3 h with stirring under protection of N$_2$ (Chen et al., 2007; Liufu et al., 2005).

2.2.3 Preparation of PAA-Fe(OH)$_3$

Fe(OH)$_3$ sol was prepared by hydrolysis as follows: Under strong stir, 50 ml deionized water was slowly dripped into 1 ml fresh prepared ferric chloride aqueous solution with the concentrate of 0.6 mol/l, then 0.5 ml acetic acid aqueous solution was also slowly dripped under the strong stir, after that, stirred the solution in boiling water bath for 1h.

In a typical polymerization process, Fe(OH)$_3$ sol 2.0 g prepared just now, acrylic acid 3 ml and deionized water 9 ml were mixed to make a solution under ultrasonic dispersing for 30 min. Then 6 mg K$_2$S$_2$O$_8$ with 9 ml deionized water were slowly dripped into the solution under stirring. The solution was deoxygenated by bubbling dry nitrogen gas for 10 min, then heated to 85 ℃ and kept for 3 h with stirring under protection of N$_2$. PAA-Fe(OH)$_3$ was forming stable suspension in water.

2.2.4 Fabrication of self-assembly films

The diazoresin (Mn≈2500g/mol) aqueous solution 0.5 mg/ml was obtained from college of chemistry and molecular engineering, Peking University. PAA-nanoparticles was dissolved in the weak alkaline aqueous solutions (pH=8) with the concentrate of 0.5 mg/ml. Surface-negatively charged quartz glass was used as the substrate. Quartz glass was first cleaned by immersed in the mixed hydrogen peroxide and concentrated sulphuric acid solution with the ratio of 3 to 7 for 24 hours and then rinsed in deionized water. Cleaned quartz glass was immersed in an aqueous solution of 0.5 mg/ml DR for 5 min, rinsed with deionized water and then dried under a stream of air. After totally dried, the quartz glass was dipped into an aqueous solution of 0.5 mg/ml PAA-CNTs for 5 min again, followed by rinsing and drying. This procedure was repeated five times to yield a 5-bilayer self-assembled ultrathin multilayer film. All stages of growth were carried out at room temperature in the dark. The fabricated films were irradiated with 200 W medium pressure mercury lamp at a distance of

25 cm for 30 S. The self-assembly process was monitored after each fabrication cycle of the films by UV-vis spectra determinations (SHIMADZU UV-1700).

2.2.5 Study of diazoresin-nanoparticle self-assembly films by AFM and FFM

A commercial atomic force microscopy (SPA400, SEIKO Co.) with Si_3N_4 cantilever was used to conduct studies of surface morphology of the thin film. The surfaces of the films were studied by the AFM with tapping mode. The images were obtained in air at 25 ℃ and the relative humidity 60 %.

Friction images in trace and retrace scan directions were recorded when the scan angle was 90º. The applied load was changed and then the friction signals recorded to study the microscopic friction of the films with different layers.

3. Results and discussion

3.1 Characterization of the PEG-CNTs

In order to obtain the evidence of the bond conversion of CNTs, the FTIR spectra are shown in Fig.1. We can see the new peaks at 846 and 950 cm^{-1} (stretching vibration of the acyl chlorides group) after the reaction from CNTs-COOH to PEG-CNTs. The absorption at 1720 cm^{-1}, which is assigned to the carboxylic ester groups, increases contrasting with CNTs-COOH due to the conversion of the acyl chlorides to ester. The reaction between PEG and CNTs can be schematically represented as shown in scheme 1.
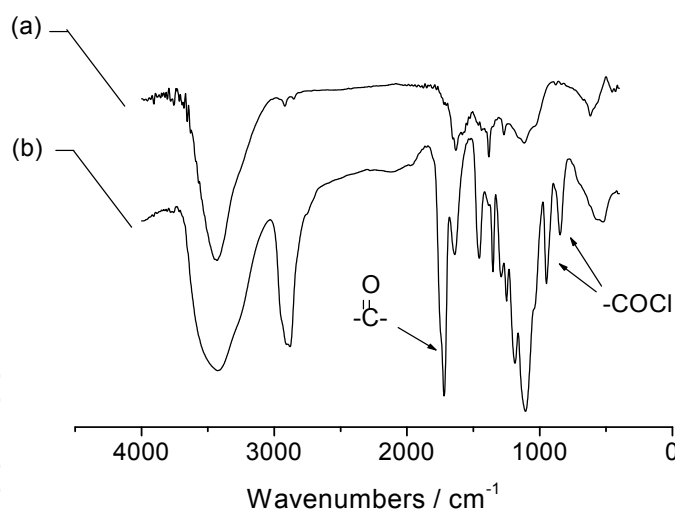
Fig. 1. FTIR spectra of (a) CNTs-COOH and (b) PEG-CNTs

3.2 Morphology of the PVA-CNT copolymer

Fig.2 displays typical TEM of the PVA-CNT copolymer. It is clear that PVA is coated on the surface of CNTs. The diameter of PVA-CNTs is much larger than that of CNTs, i.e. about 20-30 nm in diameter for CNTs and about 50-70 nm for PVA-CNTs were observed respectively. Meanwhile the much more PVA is assembled at part of curvature points of CNTs. Jia et al. also have observed similar phenomenon in the poly(methyl methacrylate)-CNT copolymer system (Jia et al., 1999). It might be proposed that CNTs had been broken in the process of
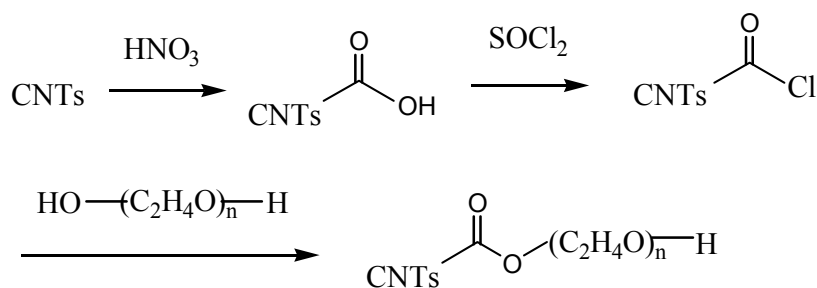
Scheme 1. Structure of CNTs conversion from carboxylic acid groups to carboxylic ester groups
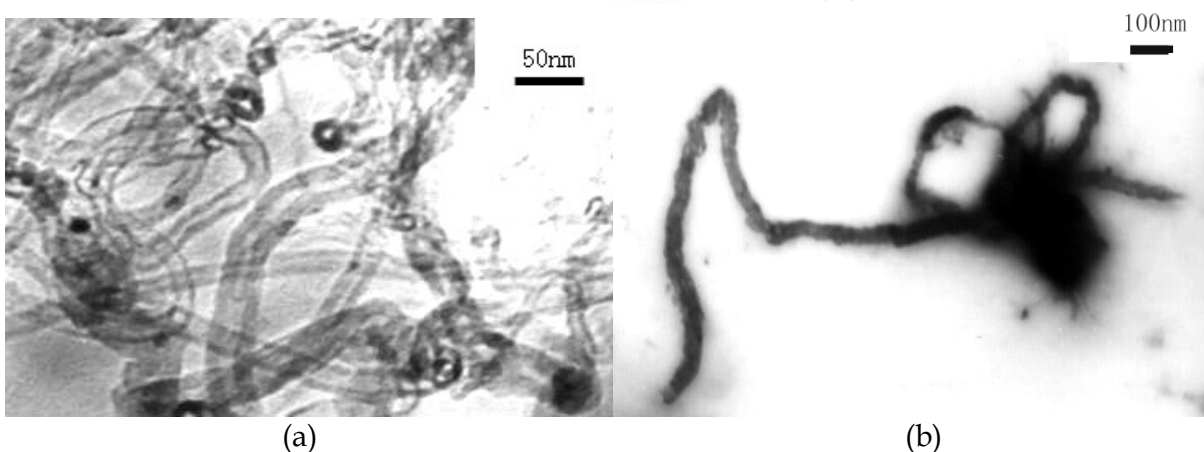

(a)   (b)

Fig. 2. Typical TEM images of (a) CNTs and (b) PVA-CNTs (Wrapping of PVA chains around CNT shell)

the reaction, because at these points structure consists of carbon atom pentagons, which is not as stable as a hexagon structure of carbon atoms. So it may be assumed that some C-C bonds at these points in CNTs can be more easily broken than other bonds, and then linked and wrapped by polymer.

3.3 Characterization of the PAM-CNT copolymer

To obtain the evidence of the bonding between the CNTs and the PAM, the PAM-CNT copolymer was characterized by FTIR, UV-visible absorbance spectra, fluorescence spectra and TEM.

FTIR spectra of the PAM-CNTs are shown in Fig.3. There is a peak at 1650 cm^{-1} (Fig 3b), which is attributed to the stretching vibration of the $-CONH_2$ group. In the spectra of CNTs in Fig3a, peaks at 1500-1700 and 3500 cm^{-1} are attributed to C=O and –OH functional groups from the acid treatment. The absorbencies of PAM-CNTs and PAM in the region of 1000 and 1500 cm^{-1} are different. The formation of these peaks may be proposed that deflections had occurred to the C-C bond (at about 1000 cm^{-1}) and the >C=O (at about 1500 cm^{-1}) on PAM-CNTs due to the existence of a chemical bond between the PAM and CNTs. The UV-visible absorption spectra and the fluorescence spectra for PAM-CNTs prepared above and PAM were measured (Fig.4). The peak at 195 nm split into two peaks on the UV-visible spectra of the PAM-CNTs. When the PAM-CNTs are excited at 347 nm, it emits fluorescence with a peak maximum at 430 nm, and increases in intensity in copolymer, but the fluorescence
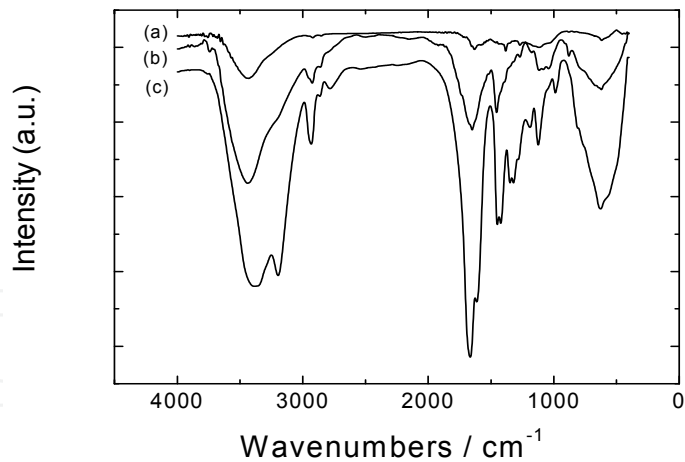
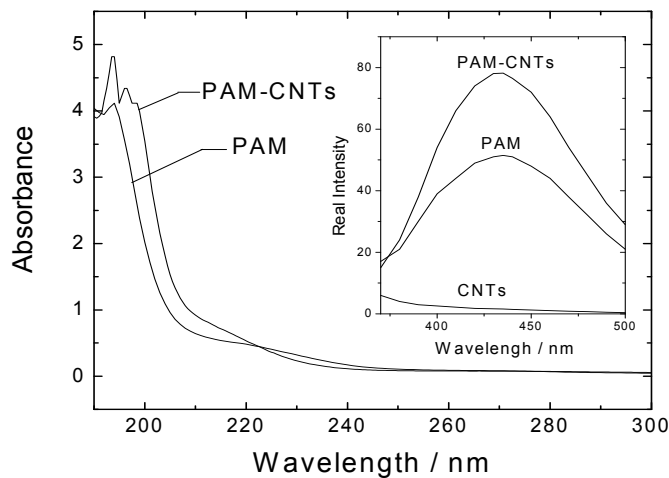Fig. 3. FTIR spectra of (a) CNTs (b) PAM-CNTs (c) PAM

Fig. 4. UV-visible absorbance spectra with PAM and PAM-CNTs. Fluorescence spectra of CNTs, PAM and PAM-CNTs (Emission spectra under 347 nm irradiation)

spectral profile of the CNT sample is not fluorescent. Sun et al. also have observed that pristine CNTs are not luminescent and the functionalization facilitates the exhibition of luminescence from CNTs via the dispersion of the nanotubes. For fullerenes, another cage-like form of carbon, multiple functionalized derivatives also are more fluorescent (El-Hami & Matsushige, 2003). CNTs are long, slender fullerenes where the walls of the tubes are hexagonal carbon (graphite structure) and often capped at each end. Mechanistically, the luminescence from CNTs was explained in terms of two possibilities: the existence of extensive conjugated electronic structures and the excitation energy trapping associated with defects in the nanotubes (Riggs et al., 2003). The solubilization of CNTs via linking PAM might contain extended π-electronic structures that are isolated as a result of nanotubes surface modification. It may be supposed that the bonds in CNTs were opened in the reaction, and CNTs can be linked with PAM by their opened π-bonds too.

Fig.5 displays typical TEM images of the PAM-CNT and CNT samples. It is clear that PAM is coated on the surface of CNTs. The diameter of PAM-CNTs is much larger than that of CNTs, i.e. about 20-30 nm in diameter for CNTs and about 100-150 nm for PAM-CNTs were observed respectively. Meanwhile the CNTs in the PAM-CNTs are much shorter than the pristine CNTs samples.
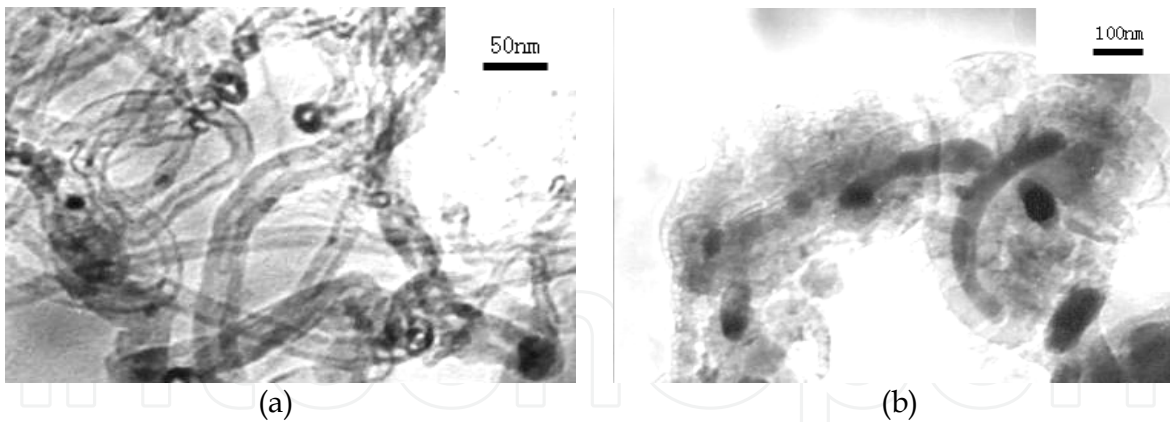
Fig. 5. Typical TEM images of (a) CNTs and (b) PAM-CNTs (Wrapping of PAM chains around CNTs shell)

3.4 Tribological and microtribological behavior of polymer-CNT nanocomposits

3.4.1 Effect of the PEG-CNT

The PB value represents the load-carrying capacity of the lubricant. The PB values of the two kinds of base stock described above containing different concentrations of PEG-CNTs are shown in Fig.6. With the increasing of the PEG-CNTs in the fluid, the load carrying capacity of the fluid is increased to a concentration of 0.5 wt.%, and then decreased. The WSD represents the anti-wear capacity of the lubricant. It is seen that the addition of the PEG-CNTs can decrease the WSD of the base stock. When the PEG-CNT content reach 0.5 wt.%, the WSD is minimum to 0.68 mm and the PB is maximum to 340 N. As a result, the obvious effects of PEG-CNTs added in the water base fluid are discovered. This infers that PEG-CNTs have pretty good load carrying and anti-wear performance in water fluid and its properties of lubrication is not proportional to its content. Since a higher concentration of PEG-CNTs makes the solution less mechanically stable, the decrease at 0.8 wt.% of PEG-CNT concentration could properly be due to the part of the PEG-CNT sediment in the tribological experiment at 1450 rpm rotating speed.
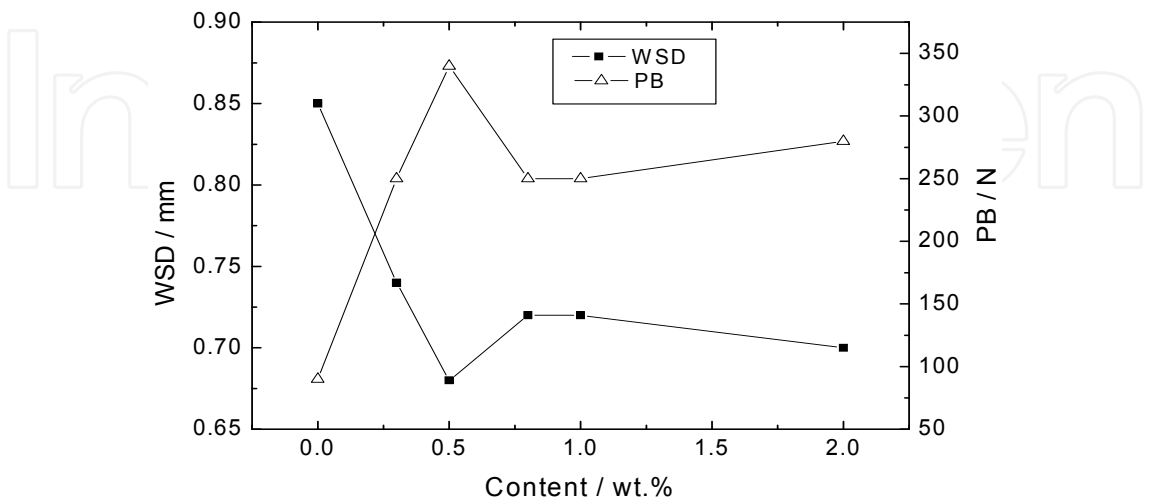
Fig. 6. Effect of the PEG-CNT content on maximum non-seized load (PB) and wear scar diameter (WSD, 30 min under a load of 200 N)

The dependence of WSD on load is shown in Fig.7. Under testing loads, the WSDs of the two kinds of base stock with 0.5 wt.% PEG-CNTs are smaller than those with 0.5 wt.% PEG, especially, at the load of 400 N, the difference in WSD between the PEG-CNTs and PEG is larger, which may be attributed to the lower load-carrying capacity of the PEG. At same time it means that the presence of CNTs can strengthen the wear resistance of the water base stock.

Dependence of WSD on rubbing time is shown in Fig.7. At the testing time, the WSD of the two kinds of base stock with 0.5 wt.% PEG-CNTs is smaller than that with 0.5 wt.% PEG. Especial after 15 min friction, the difference in WSD becomes larger, which indicates further that the presence of CNTs can strengthen the anti-wear performance of the base stock.
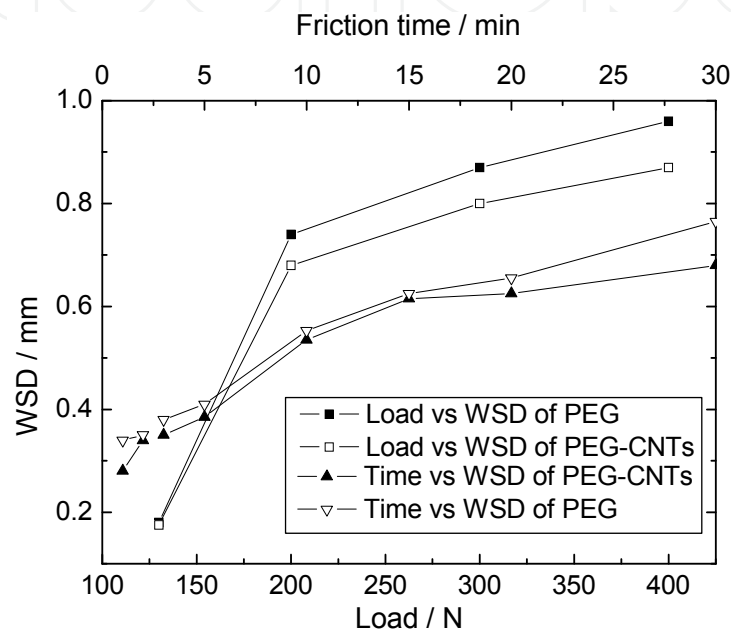
Fig. 7. Effect of load (time was 30min) and friction time (load was 200 N) on WSD (Base stock with 0.5 wt.% sample, 200 N)

In order to further study the effect of CNTs on wear and also to disclose the lubricating mechanism of CNTs, the worn surface in four-ball machine testing, which was obtained under a load of 200 N and a testing time of 30 min, was observed by optical microscopy. The wear scars of the base stock with 0.5 wt.% PEG-CNT nanocomposites and that with 0.5 wt.% PEG are shown in Fig. 8. They indicate that the wear scar obtained with the CNT nanocomposites additive is obviously smaller and exhibits mild scratches. Compared with the worn surfaces, it can be seen that the nanocomposite PEG-CNTs is relatively smoother than PEG. In other words, the PEG-CNT nanocomposites can improve microcosmic wear condition, Lei et al. have observed similar phenomenon in their fullerene-styrene sulfuric acid nanocomposite system (Lei et al., 2002). It is supposed that CNTs penetrate into the interface during friction process, and they have the possibility to cause microcosmic rolling effect between two rubbing surfaces as nanometer tiny tube. So the anti-wear abilities of the base fluid can be improved. Since CNTs have very high load-carrying capacity and the CNT nanocomposites is nanometer tiny structure, which can penetrate into rubbing surfaces and deposit there, it is reasonable to speculate that the polymer-CNTs maybe more effective than its corresponding homopolymer to support and isolate two relative motion surfaces, and therefore, the anti-wear performance of the base stock was improved.

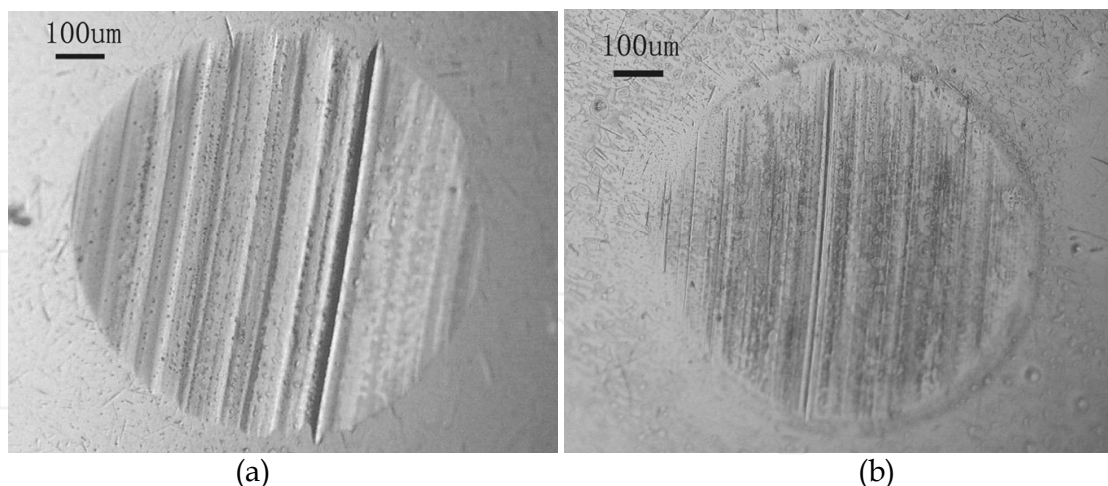(a)   (b)

Fig. 8. The morphology of worn surface (under load of 200 N and testing time of 30 min). (a) lubricated with 0.5 wt. % PEG; (b) lubricated with 0.5 wt. % PEG-CNTs

To study surface morphology and microtribological properties of thin film on a micro nanoscale, AFM/FFM is considered an excellent tool (Theoclitou et al., 1998). The surface roughnesses of PEG and PEG-CNT thin films on mica were visualized using AFM in tapping mode, shown in Fig.9. The data of RMS of PEG and PEG-CNTs are 2.244 and 12.865 nm respectively. The RMS revealed the both films are flat. The CNTs are dispersed well in the thin film and no apparent aggregation can be seen in the figures. Islands with diameter of 80-150 nm (Fig.10b) are distributed uniformly. And then it is observable that PEG film is rather flat and uniform compared to the PEG-CNT nanocomposite film. We presume that the intrinsic molecular chains are locally disordered in the CNTs-containing nanocomposites, and the existence of interpenetrating structure between the polymer phase and CNT phase.

We assume that the soft PEG chains as a matrix have reasonable anti-wear properties. Meanwhile the existence of rod and rigid segments of CNTs dispersed in thin film is expected to be beneficial for bearing the applied loads. The investigation of the relation between friction force and load could help the interpretation of AFM/FFM images at the molecular level. Fig.10 shows the overlap of two different friction forces versus load curves obtained from PEG-CNT and PEG films respectively. It is observed that both films exhibit stable and lower friction force signals below the 100 nN load due to polymer soft chains and flat surface. However, after load of 120 nN, the difference in friction force signals between the two films is larger, which may be attributed to the lower load carrying capacity of the PEG. The slopes of linear fit of PEG-CNTs and PEG in the friction signals versus load are 1.23 and 2.03 respectively, which represents the friction coefficient of the films. The friction coefficient decreased significantly as the CNTs addition. Obviously, the PEG-CNT nanocomposite film is better in bearing load and anti-wear than that of PEG film. The stability of the film can be attributed to the additional load-bearing ability afforded by CNTs chemically bonded on the nanocomposite chains.

The microtribological properties of the PEG-CNT films measured here are consistent with our perspective of CNTs-containing nanocomposites as potentially solid lubricant films, and that should encourage the idea that polymer-CNT films can be lower in friction and wear at the micro-scale.
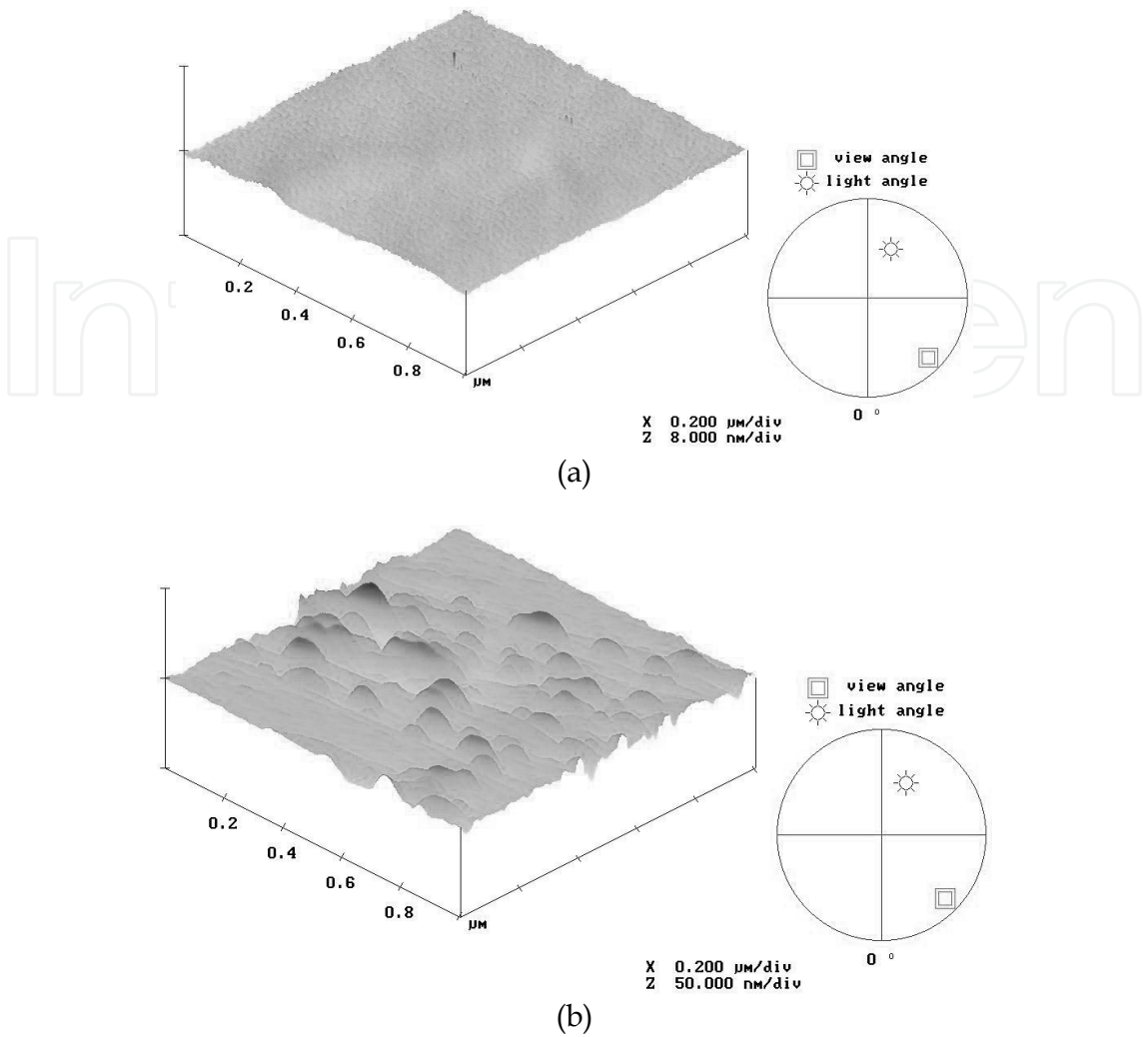
(a)

(b)

Fig. 9. Tapping mode AFM images of the spin casting films. Topographic picture of 1µm×1µm. (a) PEG film (b) PEG-CNT film
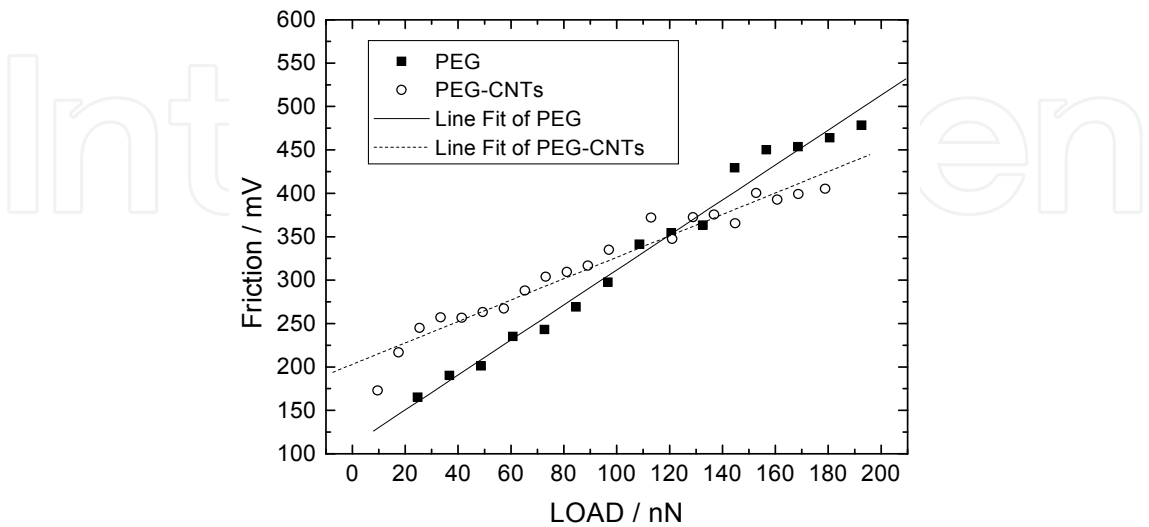

Fig. 10. Diagrams of frictional force signal versus load for PEG-CNT and PEG spin casting films

3.4.2 Effect of the PVA-CNT

The PB values of the two kinds of base stock described above containing different concentrations of PVA-CNTs are shown in Fig.11a. With the increasing of the PVA-CNTs in the fluid, the load carrying capacity of the fluid is increased to a concentration of 0.25 wt.%, and then decreased. The WSD represents the anti-wear capacity of the lubricant. The WSD data are given in Fig.11b. It is seen that the addition of the PVA-CNTs can decrease the WSD of the base stock. When the PVA-CNT content reach 0.25 wt.%, the WSD is minimum to 0.379 mm and the PB is maximum to 610 N. As a result, the obvious effects of PVA-CNTs added in the water base fluid are discovered. This infers that PVA-CNTs have pretty good load carrying and anti-wear performance in water fluid and its properties of lubrication is not proportional to its content.
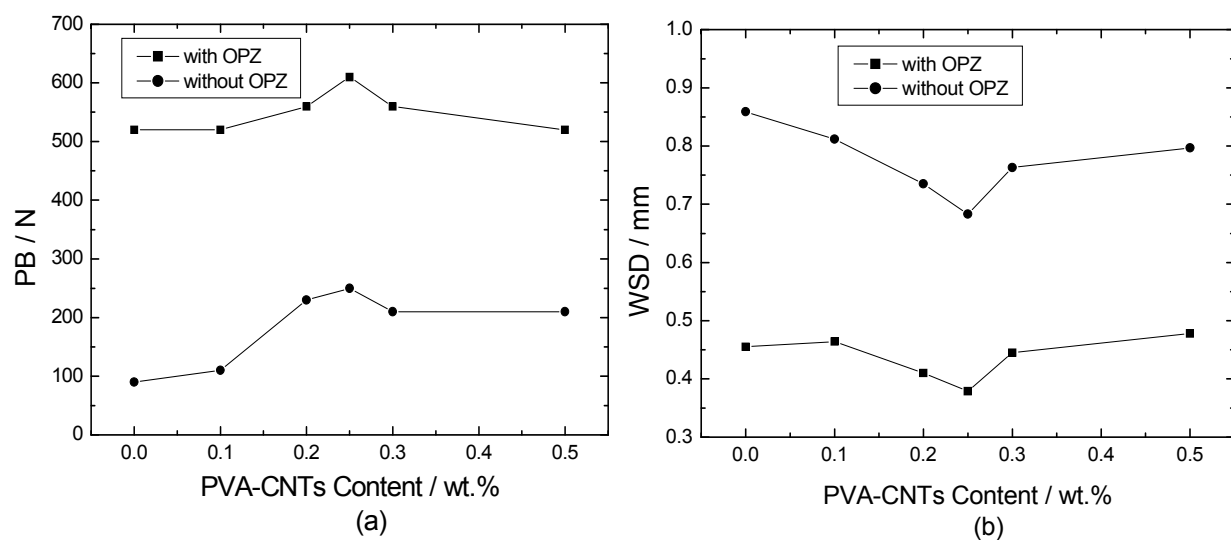
Fig. 11. Effect of the PVA-CNTs content on (a) maximum non-seized load (PB) and (b) wear scar diameter (WSD)

The dependence of WSD on load is shown in Fig.12. Under testing loads, the WSD of the two kinds of base stock with 0.25 wt.% PVA-CNTs are smaller than those with 0.25 wt.% PVA, especially, at the load of 400 N, the difference in WSD between the PVA-CNTs and PVA is larger. It means that the presence of CNTs can strengthen the wear resistance of the water base stock.

Dependence of WSD on friction time is shown in Fig.13. At the testing time, the WSD of the two kinds of base stock with 0.25 wt.% PVA-CNTs is smaller than that with 0.25 wt.% PVA. Especial after 15 min friction, the difference in WSD becomes larger, which indicates further that the presence of CNTs can strengthen the anti-wear performance of the base stock.

The worn surface of the base stock with 0.25 wt.% PVA-CNT copolymer and that with 0.25 wt.% PVA are shown in Fig.14 and 15, respectively. They indicat that the wear scar obtained with the CNT copolymer additive is obviously smaller and exhibits mild scratches. Compared with the corresponding partly enlarged micrographs of the worn surfaces, it can be seen from Fig.15 (b) that the worn surface of the copolymer PVA-CNTs is relatively smoother than that in Fig.14 (b). In other words, the PVA-CNT copolymer can improve microcosmic wear condition.
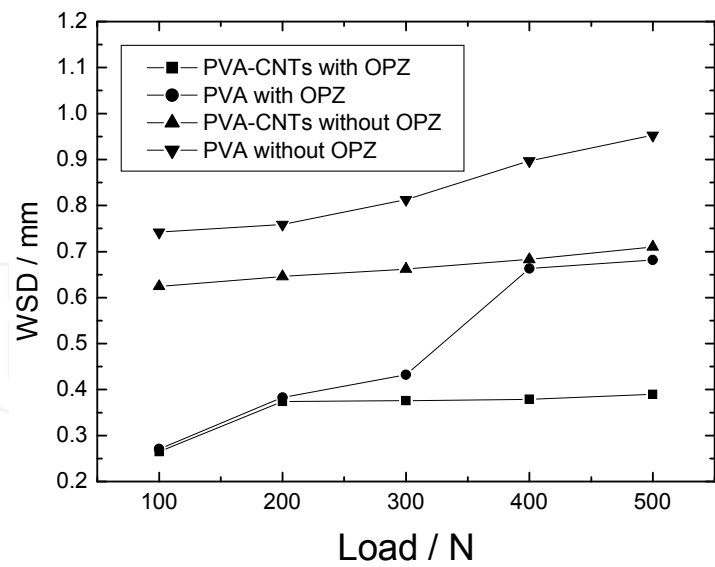
Fig. 12. Effect of load on wear scar diameter (Base stock with 0.25 wt.% sample)
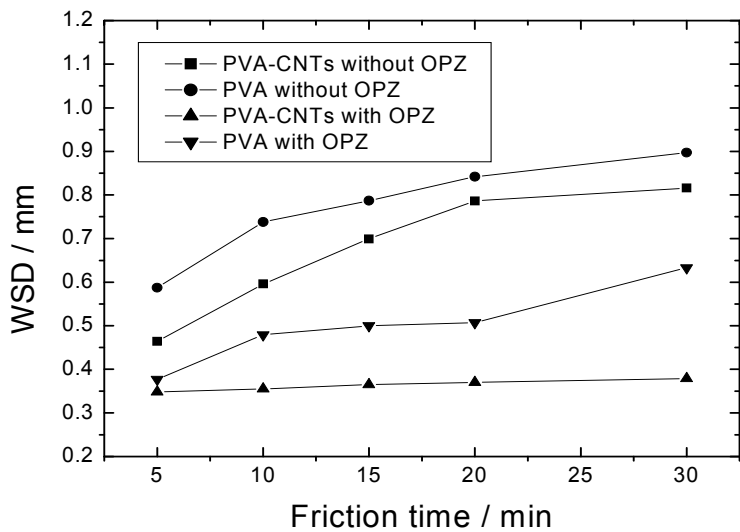

Fig. 13. Effect of friction time on wear scar diameter (Base stock with 0.25 wt.% sample)
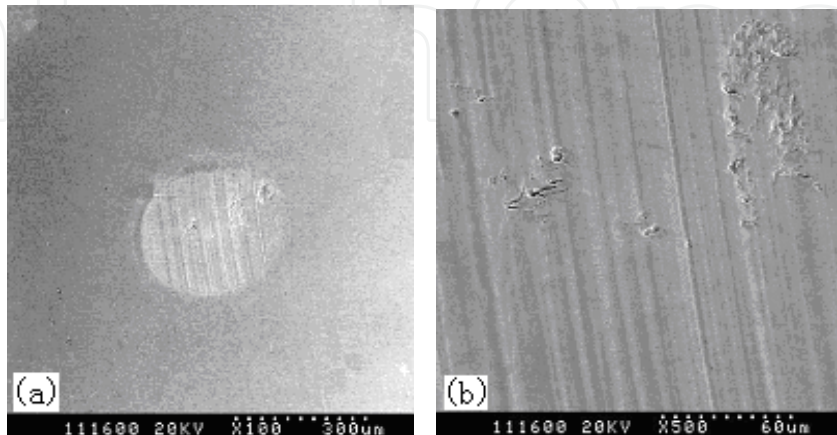

Fig. 14. SEM morphology of worn steel surface lubricated with the base stock (0.5 wt.% OPZ) containing 0.25 wt.% PVA (four-ball, 1450 rpm, 30 min, 400 N) (a) (×100) (b) (×500)
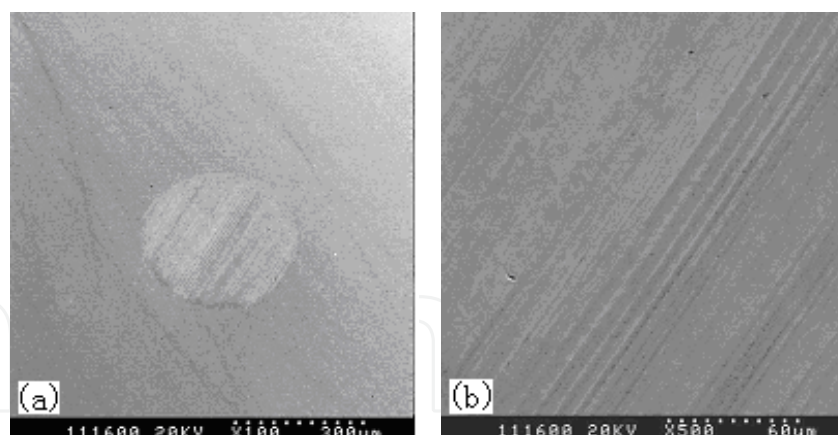
Fig. 15. SEM morphology of worn steel surface lubricated with the base stock (0.5 wt.% OPZ) containing 0.25 wt.% PVA-CNTs (four-ball, 1450 rpm, 30 min, 400 N) (a) (×100) (b) (×500)

The surface roughness of PVA and PVA-CNT composites thin films on micas was visualized by AFM in tapping mode, shown in Fig.16. The data of RMS of PVA and PVA-CNTs are 1.24 and 2.91 nm respectively, which revealed the PVA and PVA-CNT films are flat. The CNTs are dispersed uniform in PVA-CNT thin film and no apparent aggregation can be seen in the figures. And then the PVA film has a more flat and closely surface.
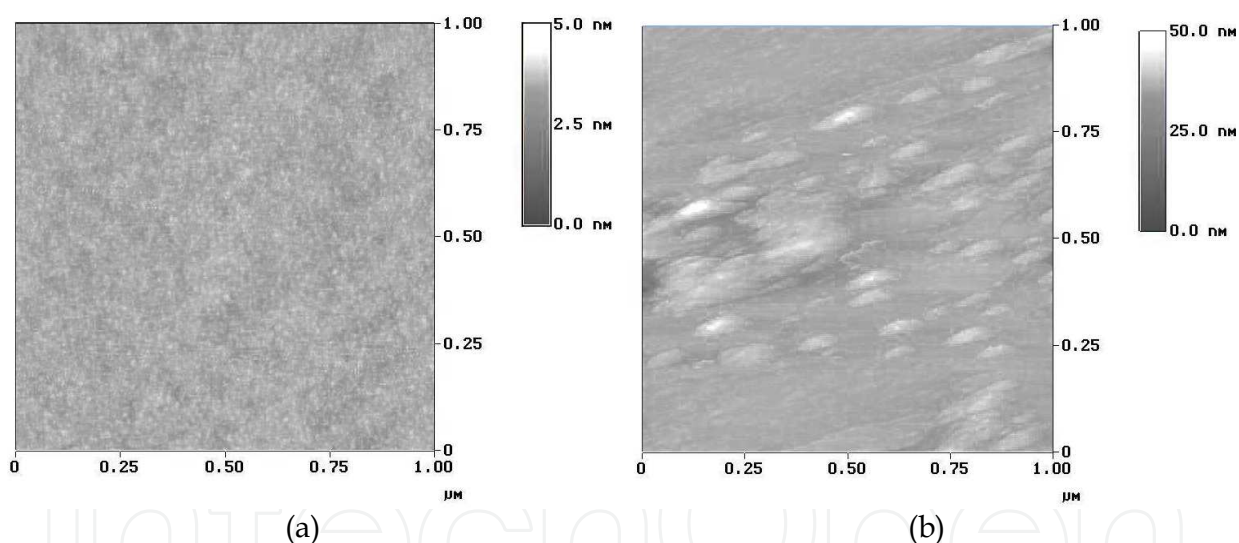
Fig. 16. Tapping mode AFM images of (a) PVA and (b) PVA-CNTs spin casting films

The friction signals of PVA-CNT and PVA films could be measured at different applied loads for the same area in the FFM map. Fig.17 shows the overlap of two different friction signals versus load curves obtained from PVA-CNT and PVA films respectively. It is observed that both films exhibit stable and lower friction signals below the 110 nN load due to polymer soft chains and flat surface. However, after load of 130 nN, the difference in friction signals between the two films is larger, which may be attributed to the lower load carrying capacity of the PVA. The slopes of linear fit of PVA-CNTs and PVA in the friction signals versus load are 1.18 and 1.82 respectively, which represents the friction coefficient of the films. The friction coefficient decreased significantly as the CNTs addition. Obviously, the PVA-CNT film is better in bearing load and anti-wear than that of PVA.
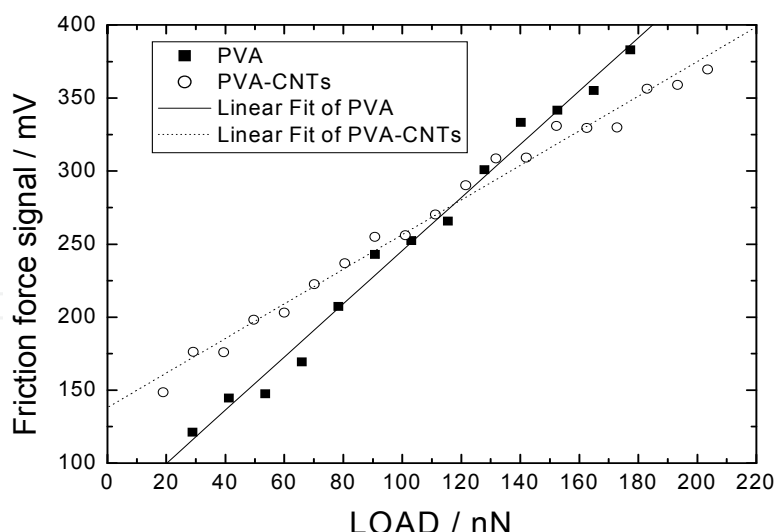
Fig. 17. Diagrams of frictional force signal versus load for PVA-CNTs and PVA spin casting films

3.4.3 Effect of the PAM-CNT

The surface roughnesses of PAM, PAM-CNT and PAM/CNT composites thin films on micas were visualized by AFM in tapping mode, shown in Fig.18. The data of RMS of PAM, PAM-CNTs and PAM/CNTs are 1.10, 2.18 and 12.44 nm respectively. The RMS revealed the PAM and PAM-CNT films are flat. The CNTs are dispersed uniform in PAM-CNT thin film and no apparent aggregation can be seen in the figures. And then the PAM film has a more flat and closely surface. In the films of physical blending samples of PAM/CNTs there are typical two separate phases and uneven surface. It also indicates that CNT surface modification disperses nanotubes uniform in polymer matrix, on the contrary, CNTs aggregation easily appears in the physical blending samples.

We assume that the soft PAM chains as a matrix have reasonable anti-wear properties. Meanwhile the existence of rigid rod-like segments of CNTs dispersed in thin films is expected to be beneficial to bearing the applied loads.

The friction signals of the blending samples films were unstable because of its uneven surface. So it was difficult to measure the microtribological properties of the films, which were coincident with their morphologies. The friction signals of PAM-CNT and PAM films could be measured at different applied loads for the same area in the FFM map. Fig.19 shows the overlap of two different friction signals versus load curves obtained from PAM-CNT and PAM films respectively. It is observed that both films exhibit stable and lower friction signals below the 130 nN load due to polymer soft chains and flat surface. However, after load of 140 nN, the difference in friction signals between the two films is larger, which may be attributed to the lower load carrying capacity of the PAM. The slopes of linear fit of PAM-CNTs and PAM in the friction signals versus load are 1.21 and 3.52 respectively, which represents the friction coefficient of the films. The friction coefficient decreased significantly as the CNTs addition. Obviously, the PAM-CNT film is better in bearing load and anti-wear than that of PAM. The stability of the film can be attributed to the additional load-bearing ability afforded by CNTs chemically bonded on the copolymer chains.
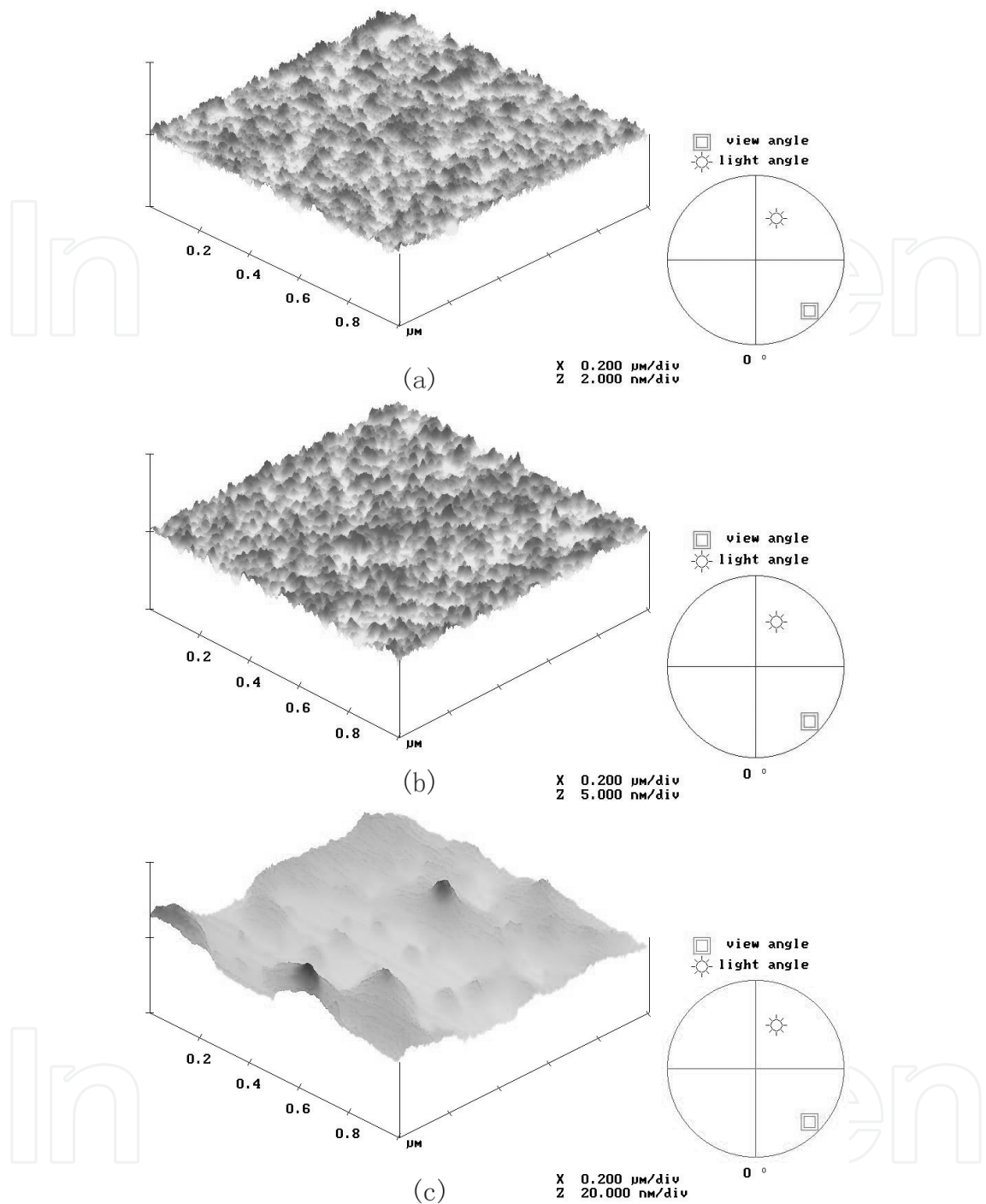
Fig. 18. Tapping mode AFM images of spin casting films. Three dimensional representation of topographic picture of 1μm×1μm. (a) PAM film (b) PAM-CNTs film (c) Physical blending sample of PAM/CNTs film

3.5 Mechanism of diazoresin-nanoparticle self-assembly films

As a cationic polyelectrolyte, DR can be easily deposited on the quartz glass surface. Then PAA-CNT deposits on the DR layer to form a DR and PAA-CNT bilayer on both sides of the quartz glass in each fabrication cycle. The absorbance of DR on quartz glass after each cyclic

deposition was recorded via a UV-vis scanning spectrometer to monitor the self-assembly process (Fig. 20). The peak at 383 nm is assigned to the absorption of the diazonium group of DR and increase linearly with increasing bilayer number. It can be seen that the absorbance increases by ca. 0.03 every two bilayers indicating smooth step-by-step deposition.
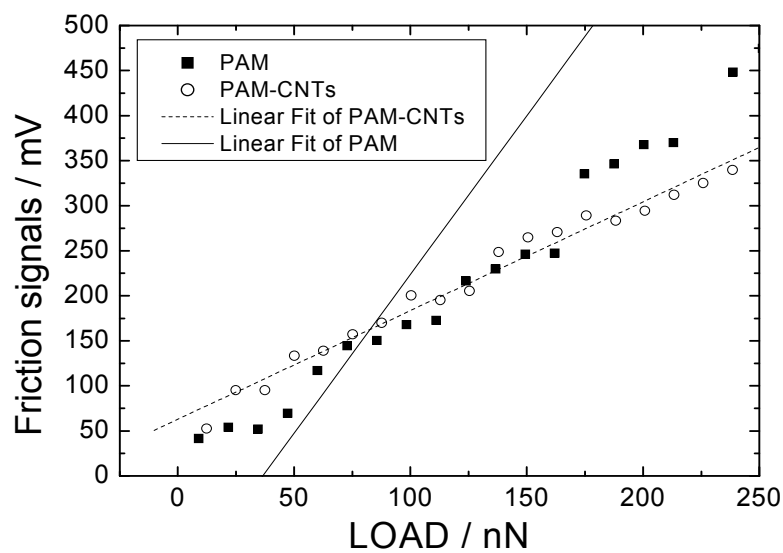
Fig. 19. Diagrams of friction signals versus load for PAM-CNTs and PAM thin films
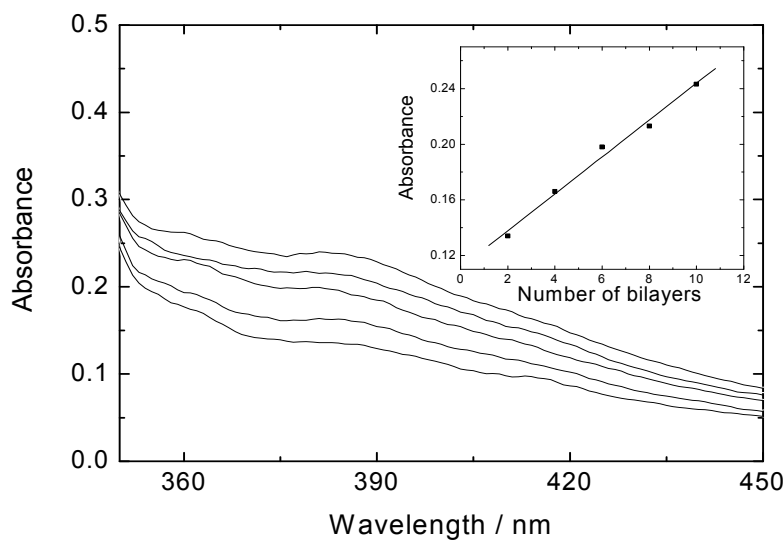
Fig. 20. The UV-vis spectra of the multilayer PAA-CNTs/DR films at 383 nm with difference numbers of bilayer, bilayer number (bottom to top): 1, 2, 3, 4, 5

The five bilayers film was then irradiated with UV light and the resulting absorbance determined. The UV-vis spectra before and after irradiation and decomposition of the diazonium groups of the films are shown in Fig. 21, respectively. The absorbance at 383 nm (diazonium group absorption) decreased with irradiation, which indicates that the ionic bonds of DR and PAA-CNTs convert partially to ester bonds. The diazonium group of the DR and PAA-CNT film decomposes easily under UV irradiation because it is sensitive towards UV light. Before irradiation, the multilayer film is formed via electrostatic attraction
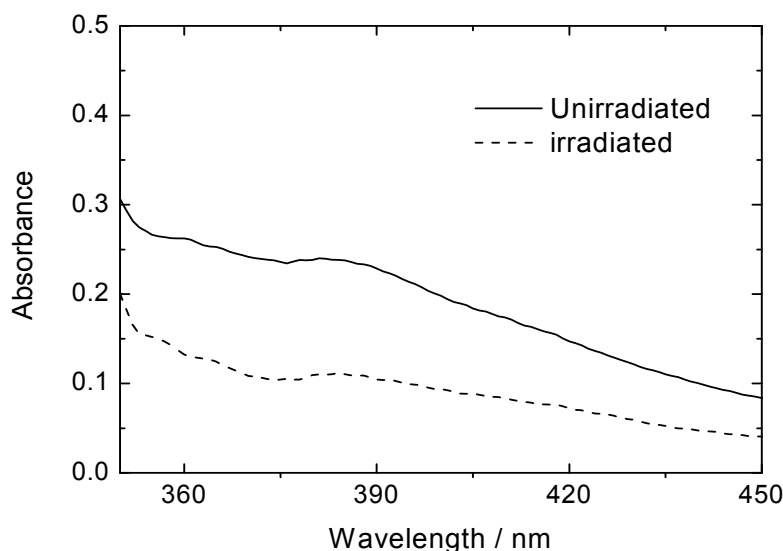
Fig. 21. UV-vis spectra of a 5-bilayer PAA-CNTs/DR film before and after UV irradiated (unirradiated and irradiated)

between the diazonium groups and carboxyl groups. Under UV irradiation, the diazonium group decomposes leading to phenyl cations, which combine with the carboxyl groups and produce covalent linkages. The conversion of the ionic bonds to covalent bonds is shown in scheme 2. This was confirmed by the FTIR studies elsewhere (Luo et al., 2001).
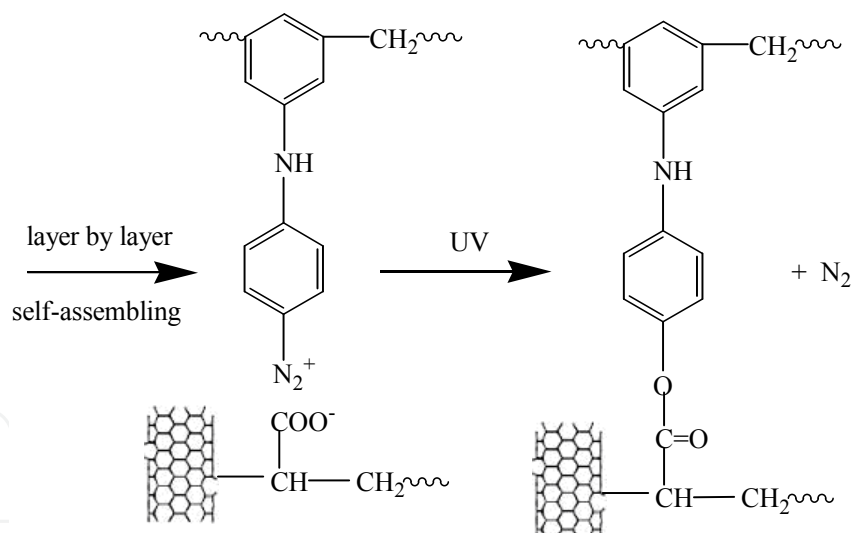
Scheme 2. The bond conversion taken place in PAA-CNTs / DR multilayer film

Under UV irradiation the films consisting of both cationic and anionic groups exhibit an extremely high tendency to aggregate by the ionic attractive force. The conversion of ionic bonds into covalent bonds makes the multilayer self-assembled films more stably packed. This is schematically represented in Scheme 3. The unirradiated films keep the original ionic structure and are much more unstable in polar solvents, such as dimethylformamide (DMF), and can be washed away. However, the irradiated films do not dissolve in DMF because of formation of the covalently crosslinked structure. The results show that the stability of the films towards polar solvents increases significantly after UV irradiation.
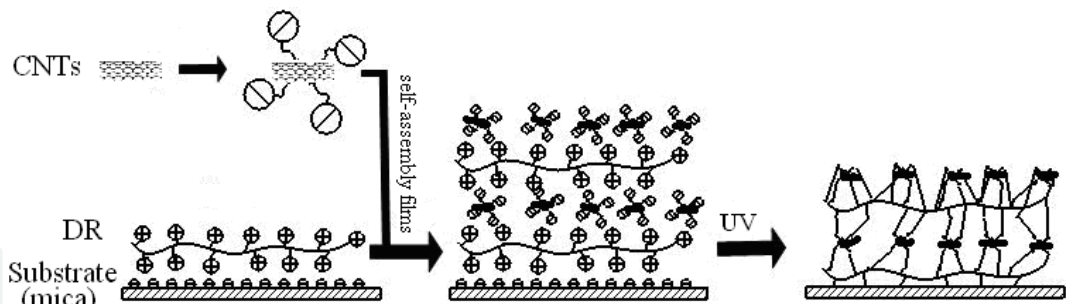
Scheme 3. Schematic diagram of the conversion of the linkage bonds from ionic to covalent in multilayer films of PAA-CNTs/DR after irradiation

Product of the TiO_2 sol was prepared by tetrabutyl titanate hydrolysis in acidic medium. TiO_2 particles were uniform and their sizes were about 50-70nm in Fig. 22. These sizes were consistent with the results of the particle size distribution analyzer (Fig. 23), and had the average diameters of 64 nm.
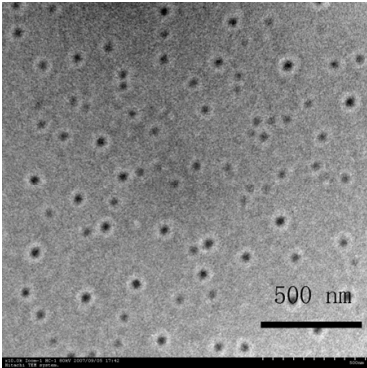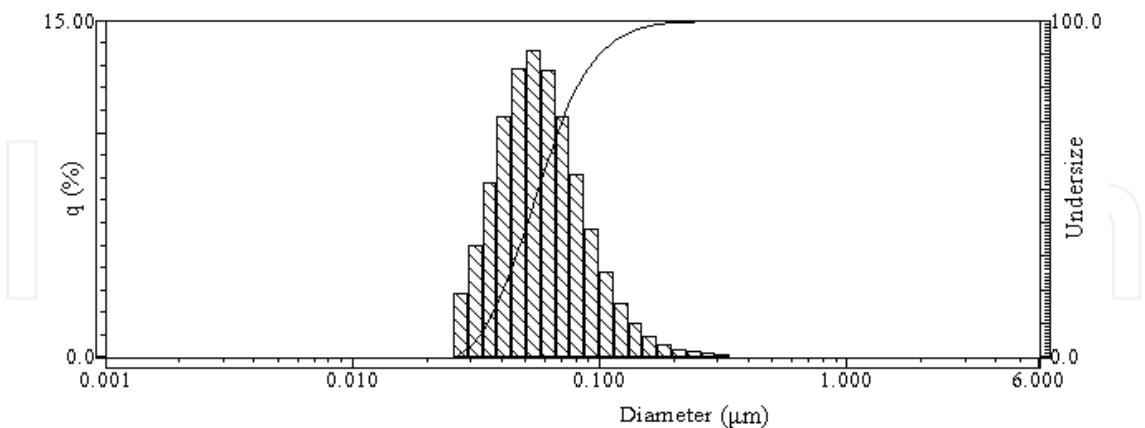

Fig. 22. TEM image of TiO_2

Fig. 23. Distribution of diameter of TiO_2 sol

PAA-TiO_2 and DR deposit on both sides of the quartz glass in each fabrication cycle. The absorbance of DR on quartz glass after each cyclic deposition was recorded via a UV-vis scanning spectrometer to monitor the self-assembly process (Fig. 24). It can be seen that the absorbance increases by ca. 0.03 every two bilayers indicating smooth step-by-step deposition.
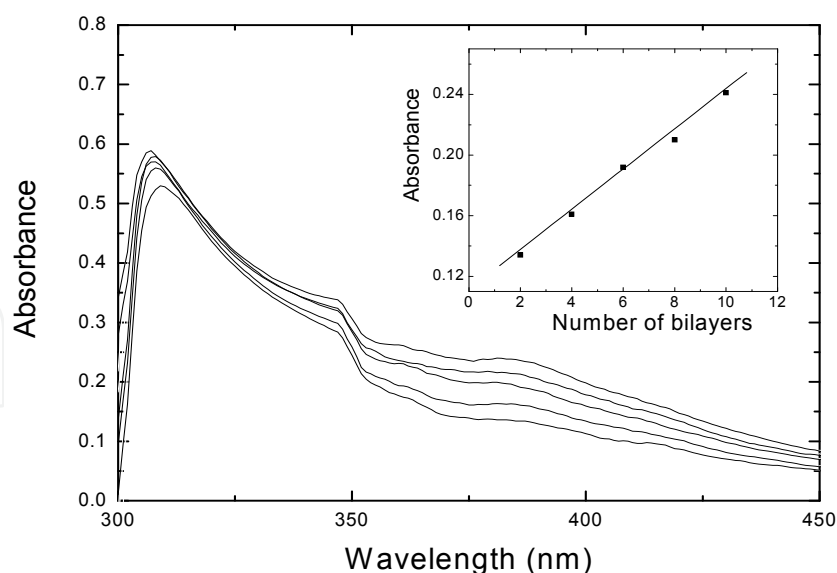
Fig. 24. The UV-vis spectra of the multilayer PAA-TiO$_2$/DR films at 383 nm with different numbers of bilayer. Bilayer number (bottom to top): 1, 2, 3, 4 and 5. Insert: Relationship between the absorbance at 383nm and the bilayer number

DR as a cationic polyelectrolyte, and PAA-Fe(OH)$_3$ solution as an anion polyelectrolyte deposits on the quartz glass in turn to form DR and PAA-Fe(OH)$_3$ bilayer films through electrostatic attraction. The absorbance of DR on the quartz glass after each cyclic deposition was recorded via a UV-vis scanning spectrometer to monitor the self-assembly process (Fig. 25). It can be seen that the peak at 383 nm which is assigned to the absorption of the diazonium group of DR increases linearly by ca. 0.06 every two bilayers. The linear relationship indicates smooth step-by-step deposition.
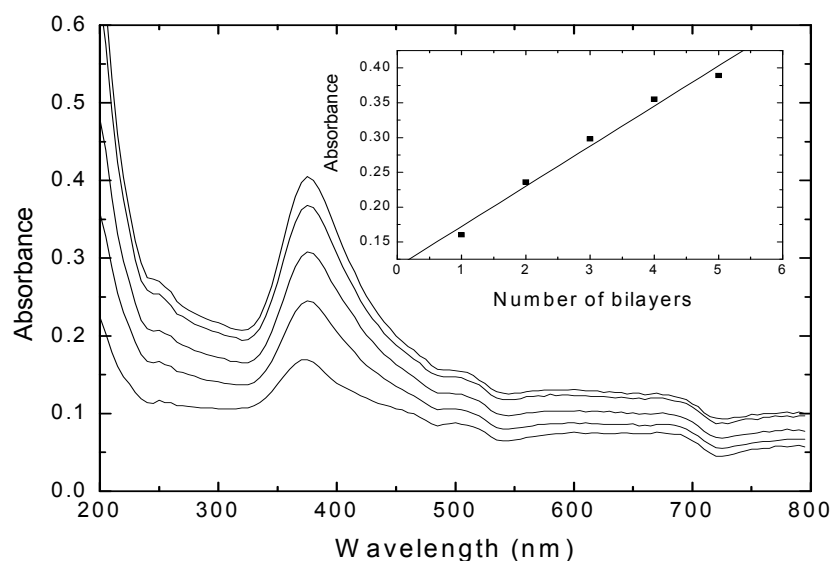

Fig. 25. UV-vis spectra of the multilayer PAA-Fe(OH)$_3$/DR films at 383 nm with difference numbers of bilayer. Bilayer number (bottom to top): 1, 2, 3, 4, 5

The UV-vis spectra of the 5-bilayer films before and after irradiation and decomposition of the diazonium groups of the films are exhibited in Fig. 26. The absorbance at 383 nm
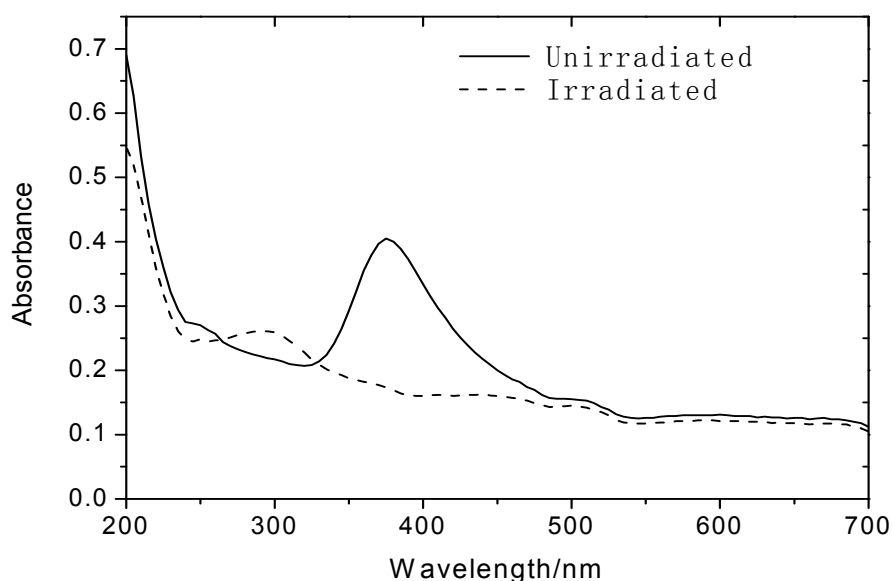
Fig. 26. UV-vis spectra of a 5-bilayer PAA-Fe(OH)$_3$/DR film before and after UV irradiated (unirradiated and irradiated)

(diazonium group absorption) decreased with irradiation, which indicates that the ionic bonds of DR and PAA-Nanoparticle converted partially to ester bonds.

3.6 Study of diazoresin-nanoparticle self-assembly films by AFM

To study surface morphology of thin films on a micro nano-scals, atomic force microscopy (AFM) is considered as an excellent tool (Sriram et al., 2009). The surface roughnesses of one layer DR film, five bilayers films of PAA-CNTs/DR and PAA-TiO$_2$/DR on micas were visualized using AFM in tapping mode, as shown in Fig. 27 (a), (b) and (c). The images reveal that the films are rather flat and uniform through the step-by-step technique. The CNTs and the particles of TiO$_2$ are dispersed well in the thin film and no apparent aggregation can be seen in Fig. 27.

AFM images with difference numbers of bilayer of PAA-Fe(OH)$_3$/DR self-assembly films (Fig.28) show surface morphology on micro-scales. The data of surface roughness of 1, 3 and 5 bilayer are 3.82, 5.47 and 8.73nm respectively. The images reveal that the films are rather flat and uniform through the step-by-step technique. The particles of Fe(OH)$_3$ are dispersed well in the thin film and no apparent aggregation can be seen.

The investigation of the relation between friction signals and load could help the interpretation of AFM/FFM images at the molecular level. A typical approach to characterize the friction properties of thin films is to investigate the friction force in the trace-retrace friction image. Fig.29 shows the friction coefficients of different number of bilayers were rather low which nearly equals to value of mica (0.0471). It is observed that the films exhibit stable and low friction signals due to polymer soft chains and flat surface. The stability of the films can be attributed to the additional load-bearing ability afforded by nanoparticles in the polymer composites. Therefore, the microtribological properties of PAA-Fe(OH)$_3$/DR self-assembly films measured here are consistent with our perspective of nanoparticles-containing polymer as potentially solid lubricant films.
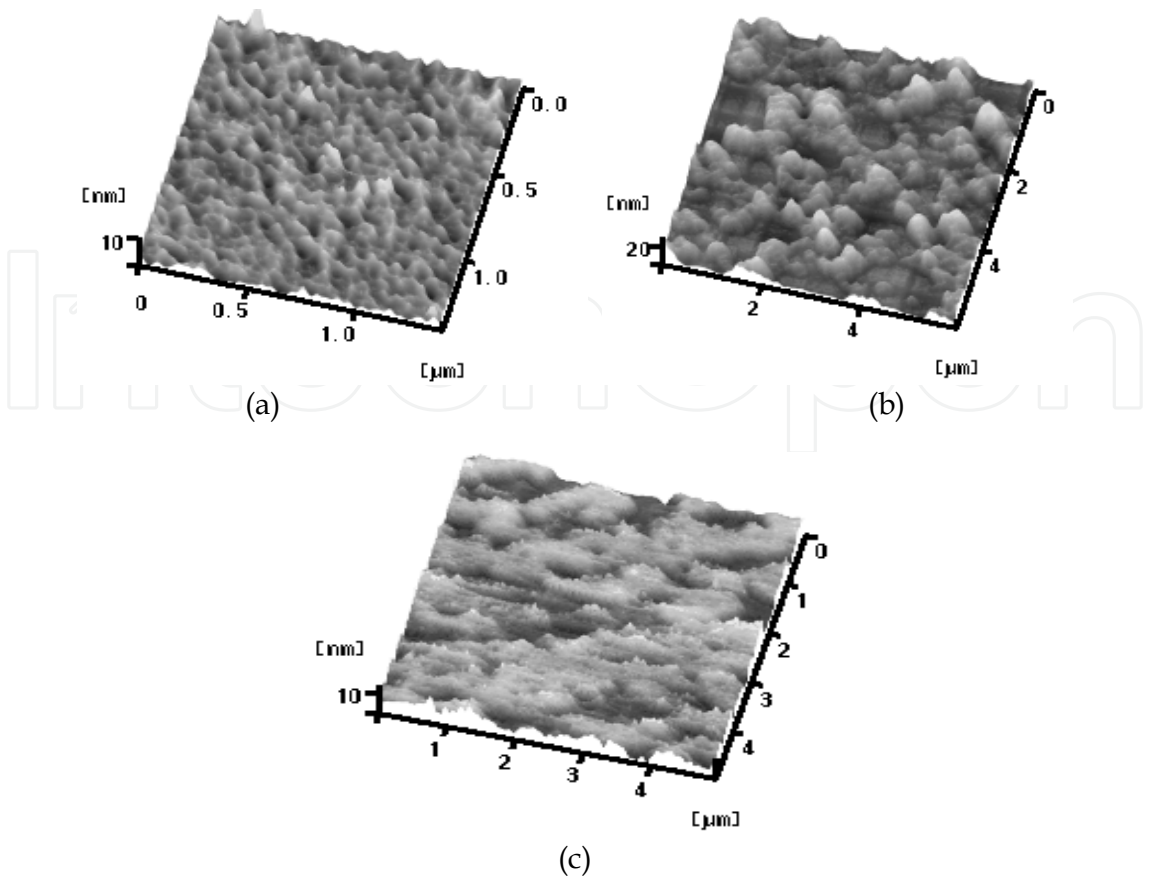
Fig. 27. AFM images of (a) 1 layer DR film, (b) 5-bilayer PAA-CNTs/DR and (c) PAA-TiO$_2$/DR film on mica surface
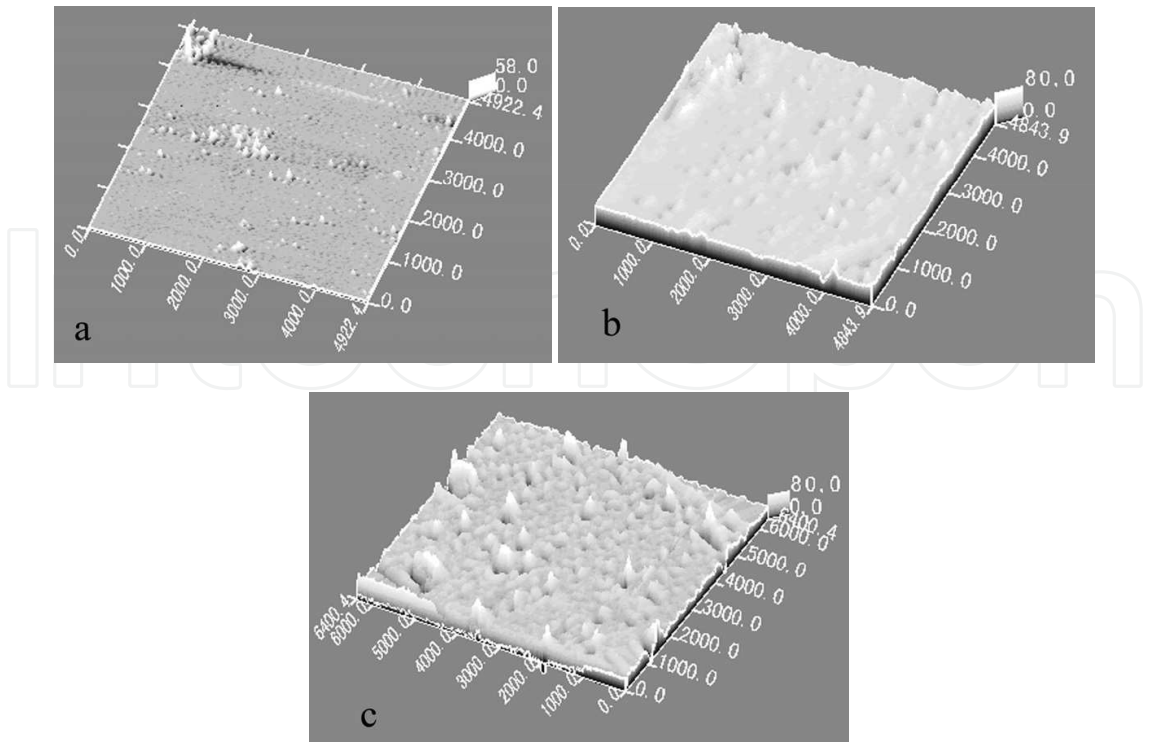

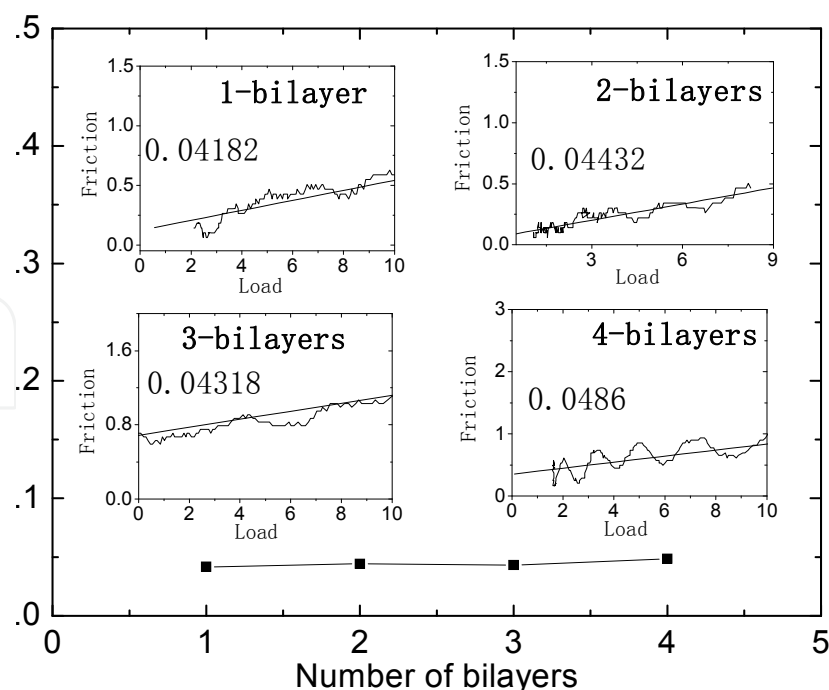Fig. 28. AFM images of films with difference numbers of bilayer, bilayer number (a to c):1, 3, 5

Fig. 29. Relationship between the friction coefficients and the bilayer number

4. Conclusion

We have succeeded in fabricated polymer-CNT nanocomposites. As a lubricant additive in water-based fluid, it can improve the wear resistance, load-carrying capacity and anti-wear ability of base stock. And then the lubrication mechanism of polymer-CNTs was deduced. The spin-casting nanocomposite thin films on mica were characterized using AFM and their height profiles were obtained. The films surface morphology is relatively flat. The difference of friction force on applied tiny load between polymer-CNT and polymer thin films are noted and discussed in terms of the role CNT segments. This supports the prediction that the load-bearing property of CNTs-containing nanocomposites thin films is enhanced.

We have succeeded in preparing PAA-nanoparticle polyelectrolytes. The multilayer thin films were fabricated on quartz glass with diazoresin as cationic polyelectrolyte and PAA-nanoparticle as anionic polyelectrolyte via the self-assembly technique, and then verified by UV-vis spectrum. The analysis of the surfaces of the self-assembly films indicate that the films are relatively flat, uniform and low friction signals.

5. Acknowledgment

6. References

Bai, T. and Cheng, X. (2006). Investigation of the Tribological Behavior of 3-Mercaptopropyl Trimethoxysilane Deposited on Silicon. *Wear*, 261(7-8): 730-737. ISSN: 0043-1648

Balani, K., Harimkar, S.P., Keshri, A., Chen, Y., Dahotre, N.B. and Agarwal, A. (2008). Multiscale Wear of Plasma-sprayed Carbon-nanotube-reinforced Aluminum Oxide Nanocomposite Coating. *Acta. Mater.*, 56: 5984-5994. ISSN: 1359-6454.

Bhushan, B., Israelachvili, J.N. and Landman, U. (2002). Nanotribology: Friction, Wear and Lubrication at the Atomic Scale. *Nature*, 374: 607-616. ISSN: 0028-0836.

Chen, J., Mamon, M.A., Hu, H., Chen, Y.S., Rao, A.M., Eklund, P.C. and Haddon, R.C. (1998). Solution Properties of Single-Walled Carbon Nanotubes. *Science*, 282: 95-98. ISSN: 0036-8075.

Cheng, X., Bai, T., Wu, J. and Wang, L. (2006). Characterization and Tribological Investigation of Self-assembled Lanthanum-Based Thin Films on Glass Substrates. *Wear*, 260(7-8): 745-750. ISSN: 0043-1648.

Chen, H.J., Jian, P.C., Chen, J.H., Wang L., and Chiu, W.Y. (2007) Nanosized-hybrid Colloids of Poly(acrylic acid)/Titania Prepared via In Situ Sol-Gel Reaction. *Ceram. Int.*, 33: 643-653. ISSN: 0272-8842.

Decher, G. (1997). Fuzzy Nanoassemblies: Toward Layered Polymeric Multicomposites. *Science*, 277: 1232-1237. ISSN: 0036-8075.

Duan, B.A. (1999). Study on Colloidal PSt-a New Type of Water-Based Lubrication Additive. *Wear*, 236: 235-239. ISSN: 0043-1648.

El-Hami, K. and Matsushige, K. (2003). Covering Single Walled Carbon Nanotubes by the Poly(VDF-co-TrFE) Copolymer. Chem. *Phys. Lett.*, 368: 168-177. ISSN: 0009-2614.

Eremenko, B.V., Bezuglaya, T.N., Savitskaya, A.N., Malysheva, M.L., Kozlov I.S. and Bogodist, L.G. (2001). Stability of Aqueous Dispersions of the Hydrated Titanium Dioxide Prepared by Titanium Tetrachloride Hydrolysis. *Colloid. J.*, 63(2): 173-178. ISSN: 1061-933X

Hiura, H., Ebbesen, T.W. and Tanigaki, K. (1995). Opening and Purification of Carbon Nanotubes in High Yields. *Adv. Mater.*, 7: 275-276. ISSN: 0935-9648.

Jia, Z., Wang, Z., Xu, C., Liang, J., Wei, B., Wu, D. and Zhu, S. (1999). Study on Poly(methyl methacrylate)/Carbon Nanotube Composites. *Mat. Sci. Eng.*, A271: 395-400. ISSN: 0921-5093.

Kim, S.H., Asay, D.B. and Dugger, M.T. (2007). Nanotribology and MEMS. *Nano today*, 2(5): 22-29. ISSN: 1748-0132.

Kwon, S.G., Piao, Y. and Park, J. (2007). Kinetics of Monodisperse Iron Oxide Nanocrystal Formation by "Heating-Up" Process. *J. Am. Chem. Soc.*, 129 (41): 12571-12584. ISSN: 0002-7863.

Li, J.W., Wang, C., Shang, G.Y., Xu, Q.M., Lin, Z., Guan, J.J. and Bai, C.L. (1999). Friction Coefficients Derived From Apparent Height variations in contact mode atomic force microscopy. *Langmuir*, 15: 7662-7669. ISSN: 0743-7463.

Lei, H., Guan, W. and Luo, J. (2002). Tribological Behavior of Fullerene – Styrene Sulfonic Acid Copolymer as Water-based Lubricant Additive. *Wear*, 252: 345-350. ISSN: 0043-1648.

Li, X.F., Guan, W., Yan, H. and Huang, L. (2004). Fabrication and Atomic Force Microscopy/Friction Force Microscopy (AFM/FFM) Studies of Polyacrylamide Carbon Nanotubes Copolymer Thin Films. *Materials Chemistry and Physics*, 88: 53-58. ISSN: 0254-0584

Li, X.F and Peng, S. (2009). Self-assembly Thin Films of Poly (acrylic acid)-Titanium Oxide. *The International Society for Optical Engineering*, 7493: 8-10. ISSN: 1022-6680

Li, X.F. and Peng, S. (2011). Poly(acrylic acid)-Ferric Hydroxide Photosensitive Self-assembly Film. *Materials Science Forum*, 663-665: 252-255. ISSN: 0255-5476

Li, X.F., Yan. H. and Peng, S. (2011). Tribological Behavior of Poly(ethylene Glycol) - Carbon Nanotubes. *Advanced Materials Research*, 217-218: 688-691.

Li, X.F, Yan, H. and Peng, S. (2011). Study of Poly(Acrylic Acid)–Carbon Nanotube Self-Assembly Films. *Designed Monomers and Polymers*, 14: 347-352. ISSN: 1385-772X

Liu, J., Rinzler, A.G., Dai, H.J., Hafner, J.H., Bradley, R.K., Boul, P.J., Lu, A., Iverson, T., Shelimov, K., Huffman, C.B., Rodriguez-Macias, F., Shon, Y.S., Lee, T.R., Colbert, D.T. and Smalley, R.E. (1998). Fullerene Pipes. *Science*, 280: 1253-1256. ISSN: 0036-8075.

Liufu, S.C., Xiao, H.N. and Li, Y.P. (2005). Adsorption of Poly(acrylic acid) onto the Surface of Titanium Dioxide and the Colloidal Stability of Aqueous Suspension. *J. Colloid. Interf. Sci.*, 281: 155-163. ISSN: 0021-9797.

Lu, C.G., Wei, F., Wu, N.Z., Zhao, X.S., Luo, C.Q. and Cao, W.X. (2004). Micropatterned Self-Assembled Film Based on Temperature-Responsive Poly (N-Isopropylacrylamide-co-Acrylic Acid), *J. Colloid. Interf. Sci.*, 277: 172-175. ISSN: 0021-9797.

Luo, H., Chen, J., Luo, G., Chen, Y. and Cao, W. (2001). Self-Assembly Films From Diazoresin and Carboxy-Containing Polyelectrolytes, *J. Mater. Chem.*, 11: 419-422. ISSN: 0959-9428.

Martínez-Martínez, D., Kolodziejczyk, L., Sánchez-López J.C. and Fernández, A. (2009). Tribological Carbon-Based Coatings: An AFM and LFM Study. *Surf. Sci.*, 603: 973-979. ISSN: 0039-6028.

Meng, H., Sui, G.X., Xie, G.Y. and Yang, R. (2009). Friction and Wear Behavior of Carbon Nanotubes Reinforced Polyamide 6 Composites Under Dry Sliding and Water Lubricated Condition. *Compos. Sci. Technol.*, 69: 606-611. ISSN: 0266-3538.

Medintz, I.L, Uyeda, H.T., Goldman, E.R. and Mattoussi, H. (2005). Quantum Dot Bioconjugates for Imaging, Labelling and Sensing. *Nat. Mater.*, 4: 435-436. ISSN: 1476-1122.

Pei, X., Hu, L., Liu, W. and Hao, J. (2008). Synthesis of Water-Soluble Carbon Nanotubes via Surface Initiated Redox Polymerization and Their Tribological Properties as Water-Based Lubricant Additive. *Eur. Polym. J.*, 44: 2458-2464. ISSN: 0014-3057.

Riggs, J.E., Guo, Z., Carroll, D. and Sun, Y.P. (2000). Strong Luminescence of Solubilized Carbon Nanotubes. *J. Am. Chem. Soc.*, 122: 5879-5880. ISSN: 0002-7863.

Shaffer, M.S.P. and Koziol, K. (2002). Polystyrene Grafted Multi-Walled Carbon Nanotubes, *Chem. Commun.*, 18: 2074-2075. ISSN: 1359-7345.

Sriram, S., Bhaskaran, M., Short, K.T., Matthews, G.I. and Holland, A. S. (2009). Thin Film Piezoelectric Response Characterisation Using Atomic Force Microscopy with Standard Contact Mode Imaging, *Micron*, 40: 109-113. ISSN: 0968-4328.

Theoclitou, M., Rayment, T. and Abell, C. (1998). *Nature*, 391: 566-568. ISSN: 0028-0836.

Tsang, S.C., Chen, Y.K., Harris, P.J.F. and Green, M.L.H. (1994). A Simple Chemical Method of Opening and Filling Carbon Nanotubes. *Nature*, 372: 159-162. ISSN: 0028-0836.

Vail, J.R., Burris, D.L. and Sawyer, W.G. (2009). Multifunctionality of Single-Walled Carbon Nanotube–Polytetrafluoroethylene Nanocomposites. *Wear*, 267: 619-624. ISSN: 0043-1648.

Yang, L.L., Yang, Z.H. and Cao, W.X. (2005).Stable Thin Films and Hollow Spheres Composing Chiral Polyaniline Composites. *J. Colloid. Interf. Sci.*, 292: 503-508. ISSN: 0021-9797.

Zhao, W.J., Zhu, M. Mo, Y.F. and Bai, M.W. (2009). Effect of Anion on Micro/nano-Tribological Properties of Ultra-thin Imidazolium Ionic Liquid Films on Silicon Wafer. Colloid. *Surface A.*, 332: 78-83. ISSN: 0927-7757.
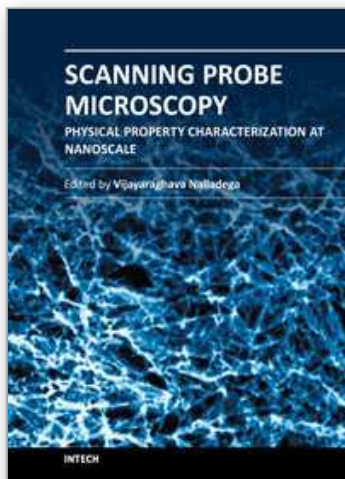
Scanning Probe Microscopy-Physical Property Characterization at Nanoscale

Edited by Dr. Vijay Nalladega

ISBN 978-953-51-0576-3

Hard cover, 242 pages

Publisher InTech

Published online 27, April, 2012

Published in print edition April, 2012

Scanning probe microscopy (SPM) is one of the key enabling tools for the advancement for nanotechnology with applications in many interdisciplinary research areas. This book presents selected original research works on the application of scanning probe microscopy techniques for the characterization of physical properties of different materials at the nanoscale. The topics in the book range from surface morphology analysis of thin film structures, oxide thin layers and superconducting structures, novel scanning probe microscopy techniques for characterization of mechanical and electrical properties, evaluation of mechanical and tribological properties of hybrid coatings and thin films. The variety of topics chosen for the book underlines the strong interdisciplinary nature of the research work in the field of scanning probe microscopy.

How to reference

In order to correctly reference this scholarly work, feel free to copy and paste the following:

INTECH

open science | open minds